The ATLAS Electron, Photon, Tau, Jet and Missing Transverse Energy High Level Trigger Algorithms Performance with first LHC Collisions

M. Wielers, for the ATLAS Collaboration

***Abstract*—Collisions of the Large Hadron Collider (LHC) were collected by ATLAS end of 2009 at a centre of mass energy of 900 GeV and are now being collected at $\sqrt{s} = 7$ TeV. This paper gives an overview of the performance of the ATLAS high level trigger for the selection of electrons, photons, taus, jets and missing transverse energy. Comparisons of the selection variables based on the calorimeter and tracking information calculated by the different trigger levels and the offline reconstruction are shown. This has been an important step in the commissioning of these triggers to ensure their correct functioning and the results from the first data are very encouraging. Furthermore, examples of comparisons between data and Monte Carlo simulations of some of the selection variables are presented. At the end a brief outlook will be given on the steps to be taken to fully commission these triggers with 7 TeV collision data.**

ATL-DAQ-PROC-2010-059
25 May 2010

I. Introduction

THE ATLAS experiment is one of the two general-purpose detectors at the LHC. Collisions were collected at the end of 2009 at a centre of mass energy of 900 GeV and since March 2010 collisions at $\sqrt{s} = 7$ TeV are being recorded. The proton-proton interaction rate at the design luminosity of $10^{34}\text{cm}^{-2}\text{s}^{-1}$ is approximately 1 GHz, while the event data recording, based on technology and resource limitations, is limited to about 200 Hz. This requires an overall rejection factor of $5 \cdot 10^6$ against minimum-bias processes while maintaining maximum efficiency for possible new physics processes. The hardware-based Level-1 (L1) trigger system uses a subset of the total detector information to make a decision on whether or not to continue processing an event, reducing the data rate to approximately 75 kHz (limited by the bandwidth of the readout system, which is upgradeable to 100 kHz). The subsequent two software-based levels, collectively known as the High-Level Trigger (HLT), are the Level-2 (L2) trigger and the Event Filter (EF). They provide the reduction to a final data-taking rate of approximately 200 Hz.

During the commissioning phase of the HLT, data were selected by the L1 trigger and subsequently processed online by the HLT, however, independent of the trigger selections all events were accepted. The HLT trigger selections are based on the identification of final state particles: electrons, photons, muons, taus, jets and missing transverse energy. The muon trigger performance is described in [1] and here only the triggers starting from a L1 calorimeter accept [2] are discussed. Seeded by the position of the objects retained at L1, the HLT algorithms are based on calorimeter and depending on the signature on tracking information. The selection according to the particle type provides efficient background rejection while maintaining a high and unbiased efficiency for the desired topologies.

In the following two sections a brief overview of the ATLAS detector and its trigger system is given. This is followed by an overview of the implementation and performance of the electron, photon, tau, jet and missing transverse energy triggers. Additional information on the commissioning of the trigger system can be found in [3].

Manuscript received May 27, 2010.

M. Wielers is with the Rutherford Appleton Laboratory, Chilton, Didcot, Oxfordshire OX11 0QX, UK (telephone: 0041 22 767 8733, e-mail: Monika.Wielers@cern.ch).

II. ATLAS Detector

The ATLAS detector is described in detail elsewhere [4]. It is composed (from the centre of the detector outwards) of the inner detector tracking detectors; a thin superconducting solenoid, generating a magnetic field of 2 T; a Liquid Argon-lead electromagnetic calorimeter; a hadron calorimeter; and a muon spectrometer system. The ATLAS detector effectively covers the angular region[1] corresponding to $|\eta| < 2.5$ for tracking and $|\eta| < 4.9$ for calorimetry (with the electromagnetic calorimeter extending up to $|\eta| < 3.2$).

As the inner detector and the calorimeters are relevant to the triggers discussed in this paper, a more thorough description of these detector systems is given here.

The inner detector tracking detector combines high-resolution detectors at the inner radii with continuous tracking elements at the outer radii. From the inside to the outside it consists of a three-layer semiconductor pixel detector, a semiconductor strip detector (SCT), and a transition radiation tracker composed of straw-tube proportional chambers interspersed with a radiator material. The expected tracking resolution is $\sigma_{p_T}/p_T = 0.05\% \oplus 1\%$.

The electromagnetic calorimeter uses lead as absorber and has an accordion geometry which results in a very good spatial uniformity with respect to the azimuthal angle, ϕ, and is divided into three longitudinal layers. It is expected to achieve an energy resolution, σ_E, given by [4] $\sigma_E/E = 10\%/\sqrt{E} \oplus 0.7\%$ where E is the energy expressed in GeV. The size of calorimeter cells depends on pseudo-rapidity and on the calorimeter layer. Layer 1 has a very fine granularity

[1]The pseudo-rapidity, η, is defined as $\eta = -\log\tan\theta/2$, where θ is the polar angle defined with respect to the beam direction.

of $\Delta\eta \times \Delta\phi = 0.003 \times 0.1$ in the barrel region and slightly coarser granularity up to $|\eta| < 2.4$. Electromagnetic showers deposit most of their energy in layer 2 which has a granularity in $|\eta| < 2.5$ of $\Delta\eta \times \Delta\phi = 0.025 \times 0.025$.

The hadron calorimeter covers the range $|\eta| < 4.9$ exploiting different techniques. The barrel calorimeter is a sampling calorimeter using iron as the absorber material and scintillating tiles as active material. In the range $1.5 < |\eta| < 4.9$ Liquid Argon calorimetry takes over: the end-cap hadron calorimeter covers $|\eta| < 3.2$ while the range $3.1 < |\eta| < 4.9$ is covered by the high-density forward calorimeter. The size of a readout cell in the hadron calorimeter is typically $\Delta\eta \times \Delta\phi = 0.1 \times 0.1$ in the Tile and hadrons end-cap calorimeter and 0.2×0.2 in the forward calorimeter. The expected resolution for measuring jets is $\sigma_E/E = 50\%/\sqrt{E} \oplus 3\%$ in $|\eta| < 3.2$ and $\sigma_E/E = 100\%/\sqrt{E} \oplus 10\%$ in $|\eta| < 4.9$.

The Minimum Bias Trigger Scintillators (MBTS), used for selecting good collision events for some of the studies shown here, cover the region $2.09 < |\eta| < 3.84$ and are mounted at $|z| = 3.6$ m between the inner tracking detector and the electromagnetic endcap calorimeter [5].

III. ATLAS Trigger System

The L1 trigger searches for high transverse-momentum muons, electrons, photons, jets, and τ-leptons decaying into hadrons, as well as large missing and total transverse energy. The selection is based on the information from a subset of detectors. High transverse-momentum muons are identified using trigger chambers in the barrel and end-cap regions of the spectrometer. Calorimeter selections are based on reduced-granularity information from all the calorimeters. Results from the L1 muon and calorimeter triggers are processed by the central trigger processor, which implements the trigger menu, which is made up of a set of triggers. If at least one trigger is satisfied the event is selected for further processing. Each of the triggers defined in the menu can, if desired, be prescaled and thus allowing an optimal use of the bandwidth as luminosity and background conditions change. Events passing the L1 trigger selection are transferred to the next stages of the detector-specific electronics and subsequently to the data acquisition via point-to-point links. In each event, the L1 trigger also defines one or more Regions-of-Interest (RoI's), i.e. the geographical coordinates in η and ϕ, of those regions within the detector where its selection process has identified interesting objects. The RoI data include information on the type of identified object and the criteria passed, e.g. a threshold. This information is subsequently used by the HLT.

The L2 selection is seeded by the RoI information provided by the L1 trigger over a dedicated data path. L2 selections use, at full granularity and precision, all the available detector data within the RoI's (approximately 2% of the total event data). The L2 menus are designed to reduce the trigger rate to approximately 3.5 kHz, with an event processing time of about 40 ms, averaged over all events. The final stage of the event selection is carried out by the EF, which reduces the event rate to roughly 200 Hz. Its selections are implemented using offline analysis procedures within an average event processing time of the order of four seconds.

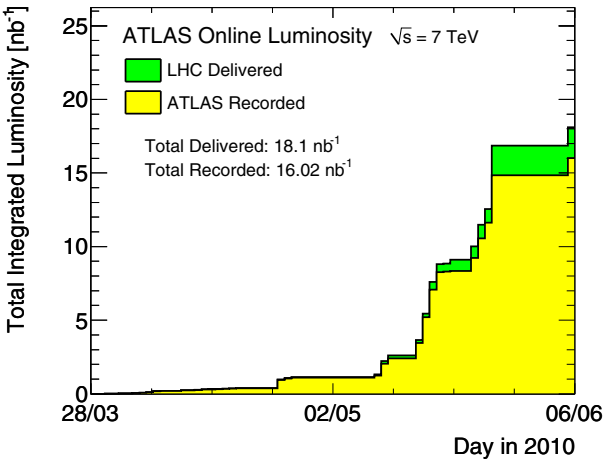

Fig. 1. Total integrated luminosity delivered by the LHC and recorded by ATLAS up to May 25, 2010

IV. Performance of the Electron, Photon, Tau, Jet and Missing Transverse Energy Trigger

The following analyses are either based on the analysis of around 9 μb^{-1} of stable beam collision data collected at $\sqrt{s} = 900$ GeV at the end of 2009 or on the first stable beam collisions taken at $\sqrt{s} = 7$ TeV (≈ 0.5 nb^{-1}) in April 2010. Up to end of May 2010 more than 10 nb^{-1} of data were recorded by the ATLAS experiment, see Figure 1.

The analysed events were required to fulfill the criteria for good collision candidates. To reject beam related background and cosmic muon event signals, the time differences between signals in the two sides of the minimum bias scintillators or the endcap electromagnetic calorimeters must be within 10 ns and 5 ns, respectively.

For Monte Carlo (MC) comparisons a sample of 10 million events of non-diffractive minimum bias events generated with Pythia, using the ATLAS tuning [6] has been used. The generated events were processed by the full ATLAS simulation and reconstruction software. For the comparisons presented here, the Monte Carlo distributions are normalised to the number of events in the data sample.

A. Overview and Performance of the Electron and Photon Trigger

At L1, photons and electrons are selected using calorimeter information with a reduced granularity. RoI's are flagged for which the L1 electromagnetic candidate is above a given threshold which subsequently seed the L2 which uses full granularity data within these RoI's. The L2 photon and electron selection deploys a fast calorimeter reconstruction algorithm and in the case of electrons also fast track reconstruction [7]. After the calorimeter and tracking reconstruction steps, so-called hypothesis algorithms are run to identify good electron and photon candidates and reject fakes coming predominantly from jet background. The selections are based on analysing the cluster shower shapes, the tracking information and cluster-track matching quantities. The EF uses the offline reconstruction algorithms but due to timing constraints bremsstrahlung

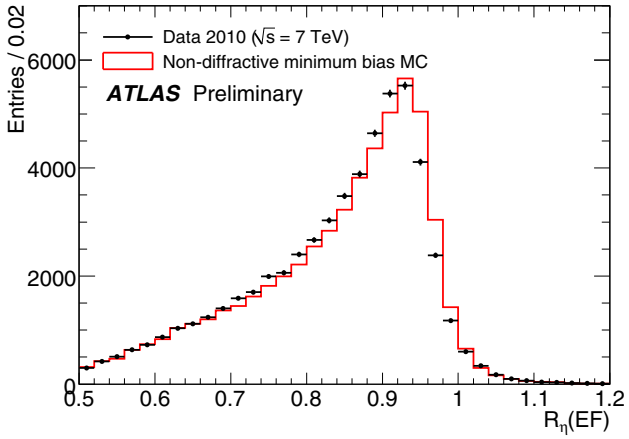

Fig. 2. Comparison of the distributions of the shower shape in η-direction R_η calculated in the second EM layer at L2 for data and simulation.

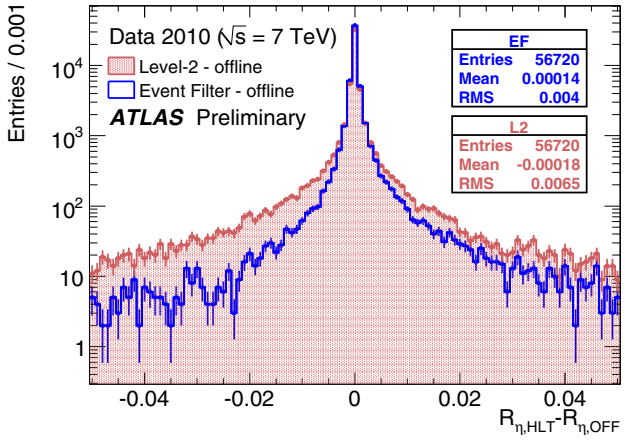

Fig. 3. Difference in R_η between the values found by the trigger and the offline reconstruction.

recovery is not applied. As at L2 the calorimeter and tracking information is explored to select good e/γ candidates. One of the important features of the HLT e/γ triggers is the use of the same or reduced set of selection criteria as used by the offline particle identification. This will ensure a minimal trigger bias in any offline physics analysis. For more information on the electron and photon trigger strategy, see [8].

For the following analysis the HLT electron and photon candidates were matched to an offline electron candidate. Matching is done in space requiring $\Delta R = \sqrt{(\Delta\eta)^2 + (\Delta\phi)^2} < 0.15$. Clusters in the complicated region between the barrel and end-cap electromagnetic calorimeter ($1.37 < |\eta| < 1.52$) and at the end of the acceptance ($|\eta| < 2.47$) have been removed.

To check the performance of the HLT electron and photon selections, candidate clusters triggered by the lowest energy L1 trigger which selects electromagnetic objects above ≈ 3 GeV have been analysed. For these objects the distributions of the selection variables have been compared at the different trigger levels with the offline distributions as well as with the expectations from MC simulations. As an example Figure 2 shows the distribution at L2 of one of the selection cuts based on $\sqrt{s} = 7$ TeV data and MC simulations. R_η is calculated based on the information in the second EM layer. This quantity is the ratio of the energy deposited in the central $\Delta\eta \times \Delta\phi = 3 \times 7$ cells divided by the energy found in 7×7 cells. This quantity peaks towards one for electrons and photons which are well contained within 3×7 cells. Note, the value of R_η can be above one due to the electronic shaping function which is set up in such a way that noise contributions will fluctuate around zero instead of producing an offset. Thus cell energies can obtain negative values which might result in the total energy deposit in $\Delta\eta \times \Delta\phi = 3 \times 7$ cells being larger than the one in 7×7 cells in case of small signals. Figure 2 shows a reasonable agreement between data and simulations. The small shift in the data to slightly lower values is also seen in the offline [9] and can be explained by cross-talk effects in this sampling. The agreement between data and MC simulations, not only in the example shown here but also for

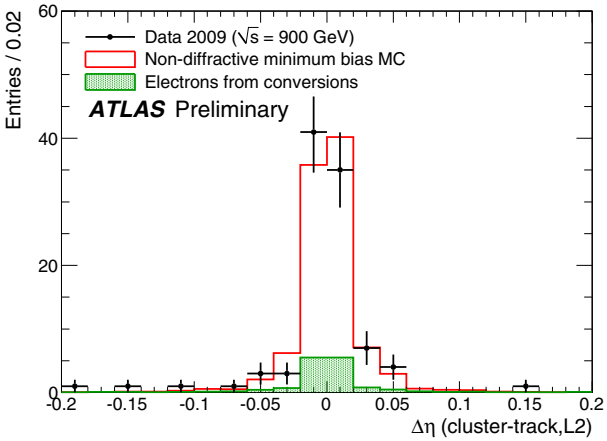

Fig. 4. Comparison of the η difference between the track extrapolated into the first EM layer and the barycentre of the cell energies in this layer calculated at L2 for data and simulation. The contribution of electrons from conversions is shown separately.

other selection criteria, has provided evidence that the initial safe and robust selection cuts developed using MC simulations are well set-up when the HLT works in rejection mode. Figure 3 shows the difference of the R_η values found in the HLT compared to the offline. It can be seen that for most clusters the trigger and offline calculations agree very well. Small differences especially at L2 for some of the clusters are caused by clusters with nearby energy deposits. In this case, it might happen that at L2 and EF slightly different cluster positions are reconstructed due to differences in the cluster finding step. Distributions for other shower shape variables, which are reported in [10], show a similar behaviour. Figure 4 shows the difference in η between the cluster and the associated track extrapolated to the calorimeter surface ($\Delta\eta$(cluster-track)) in data and simulations separately for L2 and EF. The two main components of the electron candidate sample, namely hadrons and electrons from conversions, are also shown. The distributions are reasonably well modelled. The resolutions

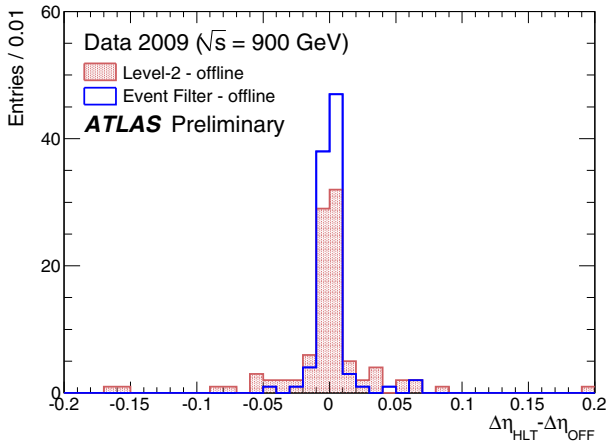

Fig. 5. Difference between $\Delta\eta$(cluster-track) found by the HLT and the offline. The distributions are shown for L2 and EF separately.

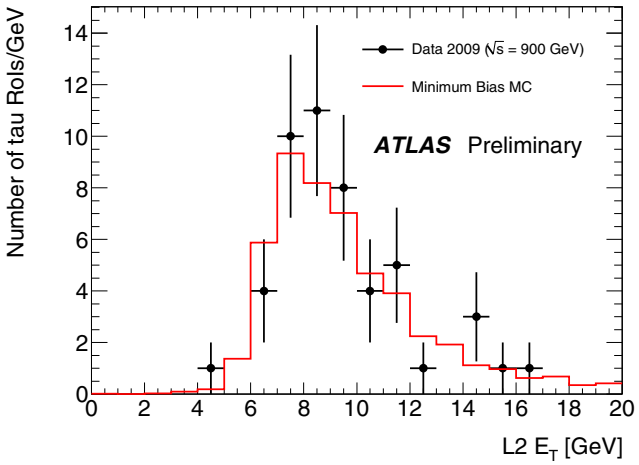

Fig. 6. Comparison of the tau candidate E_T distribution at L2 for 900 GeV data and MC simulations.

with respect to the corresponding offline distributions is shown in Figure 5. A good agreement is found between EF and offline, which is expected as the EF uses the offline tracking though no attempt for bremsstrahlung recovery is done at the EF. At L2 the resolution effects are bigger due to the differences in track reconstruction algorithm which compared to the offline is less sophisticated. Selection cuts to be used in the electron selections are therefore foreseen to be looser at this level to avoid premature losses.

B. Overview and Performance of the Tau Trigger

The tau lepton decays into electrons or muons 35% of the time, while 65% of its decays include hadrons, mostly pions. The events where taus decay into leptons can be triggered by low transverse-energy-threshold electron and muon triggers. A dedicated tau trigger has been designed to select events where a tau lepton decays into one or more hadrons. These decays can be identified by the presence of a well collimated calorimeter cluster with a small number of associated tracks.

The tau trigger is designed to select hadron decays of the tau, which are characterised by the presence of one or three charged pions accompanied by a neutrino and possibly neutral pions. At L1, the tau trigger uses the electromagnetic and hadron calorimeter trigger towers of size $\Delta\eta \times \Delta\phi = 0.1 \times 0.1$ to calculate the energy in a core and an isolation region. At L2, selection criteria are applied using tracking and calorimeter based information. This takes advantage of the narrowness of the reconstructed jet and a low track multiplicity to discriminate taus from the multi-jet background. Exploiting the same characteristics, the EF uses different selection criteria for 1-prong and multi-prong decays in more refined algorithms which are similar to the offline reconstruction algorithms. It is challenging to keep the rates for these triggers low due to the high production rate of multi-jet events. Nevertheless it is advantageous to implement tau triggers to increase the sensitivity of searches for new physics. The details of the ATLAS tau trigger are described in [8].

A clean sample of hadron tau decays is not available in the early data. Therefore the correct performance of this trigger has been checked with fake taus which are copiously produced in multi-jet events. For the analysis of the $\sqrt{s} = 900$ GeV collision data the following selection criteria were applied:

- at least one offline tau candidate reconstructed was found within $|\eta| < 2.5$
- at least one track with $p_T > 1$ GeV is associated to the tau candidate.
- the track has at least one hit in the pixel detector and six hits in the SCT.

In a data sample of 2247 events, 1249 events had at least one offline tau candidate satisfying the above mentioned requirements. A total of 1407 offline tau candidates were found in the selected events in data. Using a matching criteria of $\Delta R = \sqrt{(\Delta\eta)^2 + (\Delta\phi)^2} < 0.3$ around 50 events were matched to a L1 tau object and are available for further analysis. Figure 6 displays the L2 transverse energy (E_T) spectrum, calculated in a region of $\Delta R < 0.1$ for $\sqrt{s} = 900$ GeV data and MC simulations. A reasonable agreement between data and MC is visible. One of the selection variables for selecting good tau-candidates is the electromagnetic radius which is a measure of the shower size in $\eta - \phi$ obtained from an energy weighted ΔR of the cells associated with the tau-cluster with respect to the shower centre. The distribution of this variable is shown in Figure 7. Also here data and MC distributions give very similar results. The same holds for other variables which will be used to select tau candidates [11]. These results give confidence that the selections optimised using MC simulations will work, when the HLT applies active rejection.

C. Overview and Performance of the Jet Trigger

The ATLAS jet trigger is based on the selection of jets according to their transverse energy. The L1 jet reconstruction uses so-called jet elements, which are towers formed from the electromagnetic and hadron calorimeters with a granularity of $\Delta\eta \times \Delta\phi = 0.2 \times 0.2$. If a L1 jet candidate passes a given E_T threshold, the L2 jet trigger continues by requesting calorimeter data in a window of 1.0×1.0 around the L1 jet

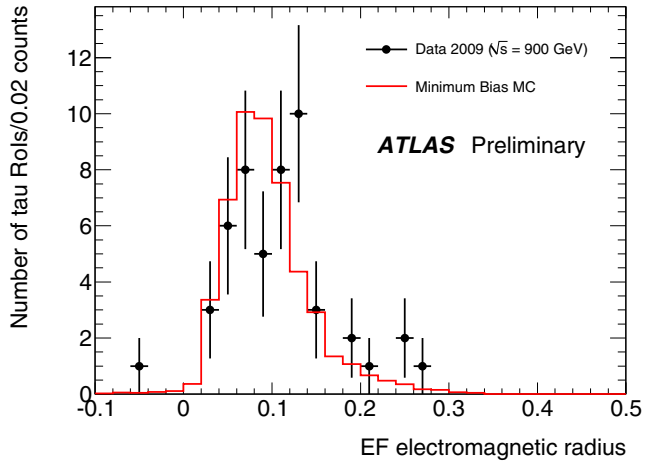

Fig. 7. Comparison of the tau candidate electromagnetic distributions for 900 GeV data and MC simulations.

RoI position and runs an iterative cone algorithm with a radius of R = 0.4 [8]. The EF jet algorithm uses a cone algorithm with R = 0.7, which is based on the offline algorithm using trigger towers formed by calorimeter cells, but configured for the online environment.

For comparison, offline jet finding starts from calorimeter towers with cells corresponding to topological clusters. These towers are the input to the anti-kt jet finder algorithm with a distance parameter of R=0.6 [8]. To further reduce the number of fake jets in the central η region, a set of quality cuts was applied on the offline jets reconstructed at the EM scale:

- $|\eta| < 2.6$
- jet $E_T > 4$ GeV
- remove jets in which the cell with maximum energy lies in the third layer of the hadron calorimeter in the crack region between the barrel and endcap calorimeter.
- remove jets in which two calorimeter cells contain more than 90% of the total jet energy
- remove jets with > 20 % energy contribution from noisy cells and problematic detector regions

For the analysis of jet triggers in the forward pseudo-rapidity regions, $3.2 < |\eta| < 4.9$, the only quality cut was that the transverse energy in the 2 cells with highest energy deposit is less than 90 %. To match the trigger with the offline jet a cut on the distance between these two jets in space is applied: $\Delta R = \sqrt{(\Delta\eta)^2 + (\Delta\phi)^2} < 0.6$. The performance of the HLT jets is assessed with respect to the offline jet definition. The relative energy resolution of the L2 jets is shown in Figure 8 for both data and MC simulation. A clear Gaussian shape is visible. Note, the jet energy is taken at the electromagnetic scale, for both L2 jets and offline jets. The mean value of the Gaussian fit indicates a shift of about 5% of the offline with respect to the L2 jets which reflects the differences between the offline and L2 jet reconstruction algorithms used. In Figures 9 and 10 the L2 and EF trigger efficiencies are shown as a function of the offline jet E_T for two different trigger thresholds. At L2 the "L2 j7" ("L2 j15") threshold refers to jets which have passed the L1 trigger and have a L2 transverse

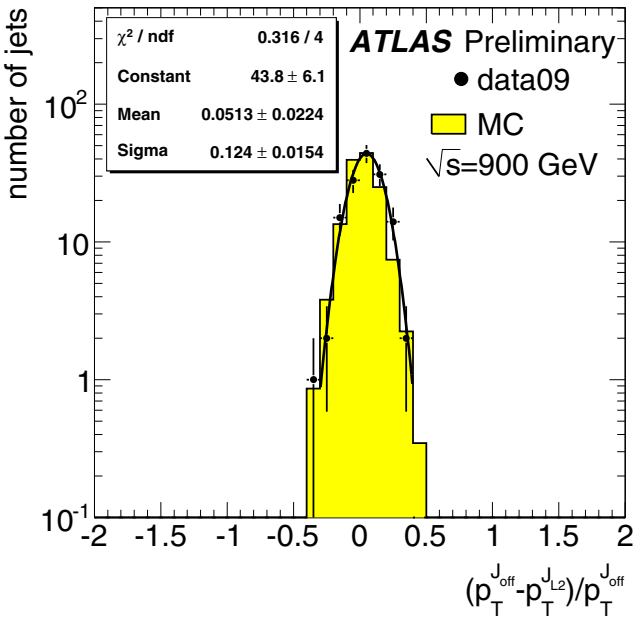

Fig. 8. Relative E_T resolution for L2 jets. The overlaid curve is the result of a Gaussian fit to the data distribution.

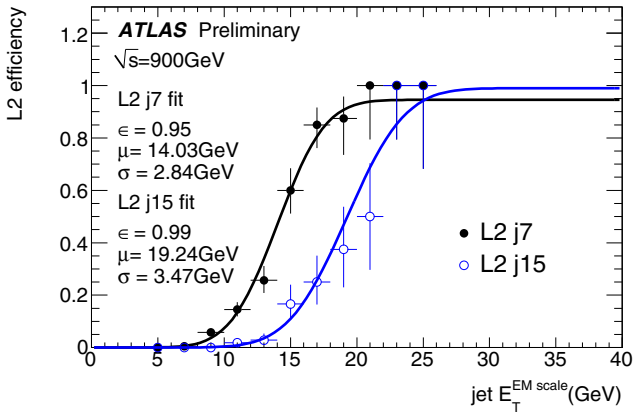

Fig. 9. L2 jet efficiency as a function of the offline jet E_T. The overlaid curve is the result of a fit (see text) to the measured distributions.

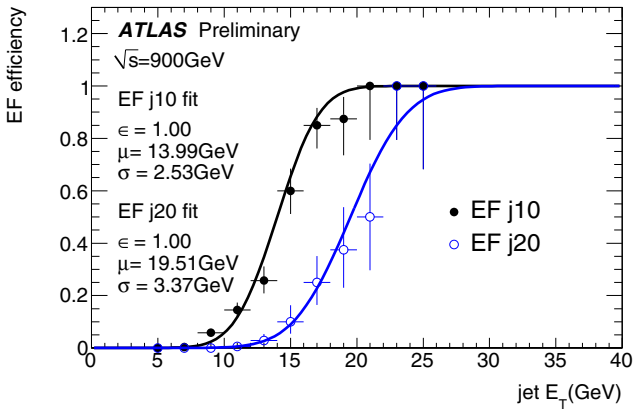

Fig. 10. EF jet efficiency as a function of the offline jet E_T. The overlaid curve is the result of a fit (see text) to the measured distributions.

energy above 7 GeV (10 GeV). Similarly, at the EF the "EF j10" ("EF j20") threshold refers to jets which have passed the "L2 j7" ("L2 j15") threshold and have an EF jet E_T above 10 GeV (20 GeV). Hadronic jet energy corrections are not applied for the L2 efficiency measurement, while for the EF jet energies a hadronic energy correction based on the energy density of the calorimeter cells derived from MC is used. [8]. The overlaid curve is the result of a fit to the measured efficiency distributions of the form

$$\text{eff}(x) = \frac{\epsilon}{2}(1 + \text{erf}(\frac{x-\mu}{\sqrt{2}\sigma})) \quad (1)$$

where ϵ represents the efficiency mid-point, μ the plateau and σ is the width of the turn-on. Figures 9 and 10 show the turn-on for data and MC simulations and also for jets a reasonable agreement between data and MC simulations is observed. More performance examples can be found in [12].

D. Overview and Performance of the Missing Energy Trigger

At L2, the missing transverse energy (E_T^{miss}) is computed by adding the vector sums of all muon momenta to the calorimetric measurement done at L1. Due to the timing constraints it is not possible to read out the cell energies of the whole calorimeter system at this level. At EF, the contributions from both calorimetry and muon spectrometer are recomputed. Only cells with a measured energy above three times the RMS of the noise are considered for the E_T^{miss} calculation. Because hadronic calibrations were not yet commissioned, the trigger output was compared with the values reconstructed offline without correcting for hadronic to electromagnetic layer differences. However, the EF algorithm include some simple layer-based hadronic calibrations, which were unfolded offline for this analysis. For the assessment of the performance, the obtained distributions in the HLT are compared to the default offline reconstructions which uses topological clustering (MET Topo) [2] [8]. These clusters are formed at the electromagnetic scale.

For the studies shown here, only events taken at $\sqrt{s} = 7$ TeV and selected by the minimum bias trigger are analysed. Figure 11 shows the correlation between the E_T^{miss} measured at the EF and the offline reference for all events for which at L1 E_T^{miss} exceeds 10 GeV. As can be seen a good correlation between the two quantities is found. A few events with high E_T^{miss} values containing jets arising from noise fluctuations could be rejected offline. The turn-on for the EF E_T^{miss} trigger selecting events above 5 and 20 GeV are shown in Figures 12 and 13 respectively. Sharp turn-on curves are visible which implies the trigger bias on the offline E_T^{miss} measurement is small. The distributions are displayed for data and MC simulations and as seen for other triggers already a good agreement between data and MC simulations is observed. More performance examples can be found in [13].

[2]Topological clusters are built starting from seed cells with an absolute value of the signal above four times the noise RMS. In the next step all neighbouring cells with energies above two times the RMS noise are added and finally all adjacent cells are added without applying any noise suppression cuts.

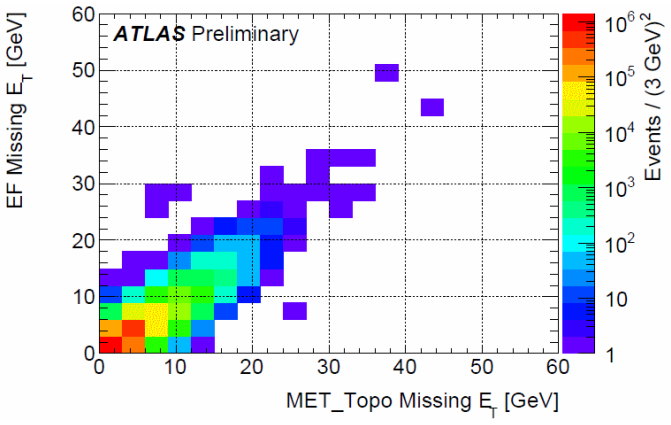

Fig. 11. Correlation between the E_T^{miss} measured at the EF and the offline for all events for which at L1 E_T^{miss} exceeds 10 GeV.

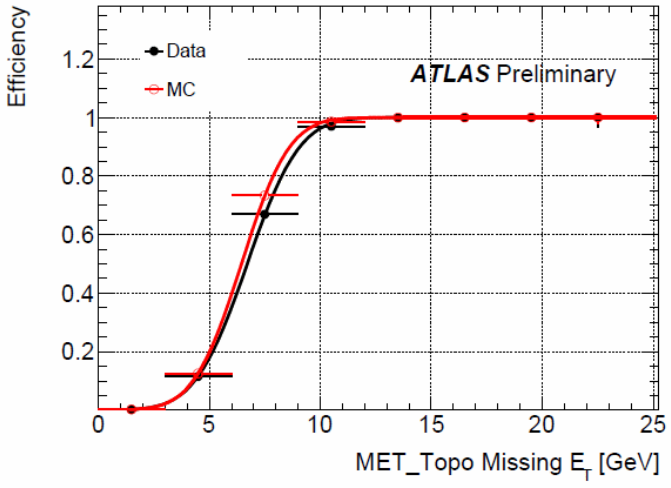

Fig. 12. Turn-on of the EF trigger selecting events with $E_T^{\text{miss}} > 5$ GeV for data and MC simulations.

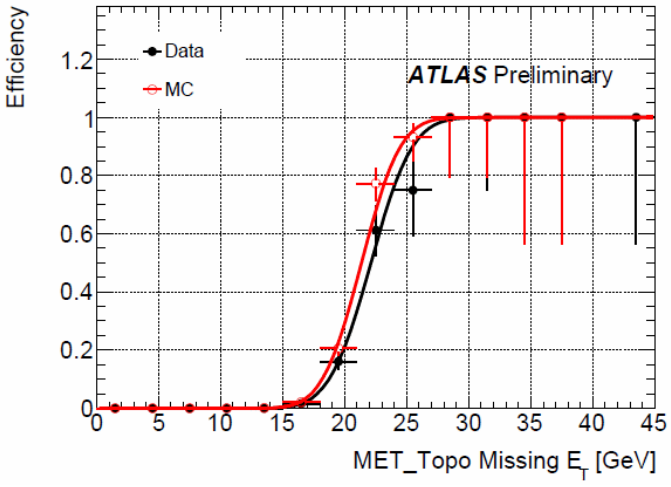

Fig. 13. Turn-on of the EF trigger selecting events with $E_T^{\text{miss}} > 20$ GeV for data and MC simulations.

V. Conclusion

During the 2009 and the 2010 LHC collision period in 2010 the HLT was run online without rejecting any events

for luminosities below approximately $10^{29}\text{cm}^{-2}\text{s}^{-1}$, as the rate of the L1 calorimeter and muon triggers was low enough to be written out directly to mass storage. In this paper the HLT selections based on the identification of final state particles: electrons, photons, taus, jets and missing transverse energy were discussed. The performance of these triggers was assessed by comparing the selection variables at the HLT with the offline reconstruction. The studies have revealed a good agreement with respect to the offline and constituted an important step in the commissioning of these triggers showing that the trigger is working correctly and that the trigger bias on the offline reconstruction is small. Comparisons between data and MC simulations showed a reasonable agreement for the selection variables at trigger level. This was the first indication that triggers foreseen for the first physics run at $\sqrt{s} = 7$ TeV, and which were optimised in a robust and safe way using simulations, are selecting electrons, photons, taus, jets and missing transverse energy as expected.

These studies were vital for preparing the HLT to start working in active rejection mode for LHC luminosities above $L \approx 2 \times 10^{29}\text{cm}^{-2}\text{s}^{-1}$. The highest L1 rate arose from the low-E_T electromagnetic triggers and, therefore, the lowest-E_T electron and photon triggers were the first ones which needed to be fully validated. The decision the triggers were ready to actively select events was partly based on the analyses shown here. When the LHC peak luminosity reached for the first time $2.1 \times 10^{29}\text{cm}^{-2}\text{s}^{-1}$ at the end of May 2010, these triggers went into active selection. With higher integrated luminosity, electrons from physics signals such as $J/\Psi \rightarrow ee, W \rightarrow e\nu$ and $Z \rightarrow ee$ will be analysed and the studies presented here will be redone. This constitutes the final validation step to ensure the selection cuts are well set-up and premature losses with respect to the offline are small.

With a further increase in luminosity more triggers will apply active HLT selection until finally the complete HLT is enabled to actively select interesting collisions and the physics program of ATLAS can be fully exploited. At this point performance measurements will be carried out on a signal enriched sample and trigger efficiencies will be determined by methods such as tag and probe using Z and J/Ψ candidates or bootstrap [8]. To prepare for even higher luminosities the trigger selections will be optimised based on the data. These studies will need to include pile-up effects.

REFERENCES

[1] The ATLAS Collaboration, M. Owen, *Commissioning of the ATLAS Muon High Level Trigger with Cosmics and Beam Collisions at the LHC*, these proceedings.

[2] The ATLAS Collaboration, J. Lundberg, *Performance of the ATLAS First-Level Trigger with First LHC Data*, these proceedings.

[3] The ATLAS Collaboration, B. Petersen, *Commissioning of the ATLAS High Level Trigger with Proton Collissions at the LHC*, these proceedings.

[4] The ATLAS Collaboration, G. Aad *et al.*, *The ATLAS Experiment at the CERN Large Hadron Collider*, JINST **3** (2008).

[5] The ATLAS Collaboration, G. Aad *et al.*, *Charged-particle multiplicities in pp interactions at $\sqrt{900}$ GeV measured with the ATLAS detector at the LHC*, Phys.Lett.B688; 21-42 (2010)..

[6] The ATLAS Collaboration, G. Aad *et al.*, *ATLAS Monte Carlo tunes for MC09*,

[7] The ATLAS Collaboration, I. Christidi, *Performance of the ATLAS Inner Detector Trigger Algorithms in p-p Collisions at Centre-of-Mass Energy of 900 GeV*, these proceedings.

[8] The ATLAS Collaboration, G. Aad *et al.*, *Expected performance of the ATLAS experiment: detector, trigger and physics*, e-Print: arXiv:0901.0512 [hep-ex], (2008)

[9] The ATLAS Collaboration, G. Aad, *Electron and photon reconstruction and identification in ATLAS: expected performance at high energy and results at 900 GeV*, ATLAS-CONF-2010-005, Geneva, (2010) .

[10] The ATLAS Collaboration, G. Aad *et al.*, *Performance of the Electron and Photon Trigger in p-p Collisions at $\sqrt{s} = 900$* GeV, ATLAS-CONF-2010-022, Geneva, (2010)

[11] The ATLAS Collaboration, G. Aad *et al.*, *Performance of the ATLAS Tau Trigger in p-p Collisions at $\sqrt{s} = 900$* GeV, ATLAS-CONF-2010-021, Geneva, (2010)

[12] The ATLAS Collaboration, G. Aad *et al.*, *Performance of the ATLAS jet trigger with pp Collisions at $\sqrt{s} = 900$* GeV, ATLAS-CONF-2010-028, Geneva, (2010)

[13] The ATLAS Collaboration, G. Aad *et al.*, *The ATLAS missing E_T trigger performance with initial LHC runs at $\sqrt{s} = 900$* GeV, ATLAS-CONF-2010-026, Geneva, (2010)